Chemistry & Biology
Article

Conversion of Red Fluorescent Protein into a Bright Blue Probe

Oksana M. Subach,[1,5] Illia S. Gundorov,[1,5] Masami Yoshimura,[2] Fedor V. Subach,[1] Jinghang Zhang,[3] David Grüenwald,[1] Ekaterina A. Souslova,[4] Dmitriy M. Chudakov,[4] and Vladislav V. Verkhusha[1,*]
[1]Department of Anatomy and Structural Biology, Albert Einstein College of Medicine, Bronx, NY 10461, USA
[2]Department of Comparative Biomedical Sciences, School of Veterinary Medicine, Louisiana State University, Baton Rouge, LA 70803, USA
[3]Flow Cytometry Core Facility, Albert Einstein College of Medicine, Bronx, NY 10461, USA
[4]Shemiakin-Ovchinnikov Institute of Bioorganic Chemistry, Miklukho-Maklaya 16/10, Moscow 117997, Russia
[5]These authors contributed equally to this work
*Correspondence: vverkhus@aecom.yu.edu
DOI 10.1016/j.chembiol.2008.08.006

SUMMARY

We used a red chromophore formation pathway, in which the anionic red chromophore is formed from the neutral blue intermediate, to suggest a rational design strategy to develop blue fluorescent proteins with a tyrosine-based chromophore. The strategy was applied to red fluorescent proteins of the different genetic backgrounds, such as TagRFP, mCherry, HcRed1, M355NA, and mKeima, which all were converted into blue probes. Further improvement of the blue variant of TagRFP by random mutagenesis resulted in an enhanced monomeric protein, mTagBFP, characterized by the substantially higher brightness, the faster chromophore maturation, and the higher pH stability than blue fluorescent proteins with a histidine in the chromophore. The detailed biochemical and photochemical analysis indicates that mTagBFP is the true monomeric protein tag for multicolor and lifetime imaging, as well as the outstanding donor for green fluorescent proteins in Förster resonance energy transfer applications.

INTRODUCTION

Green fluorescent protein (GFP) from *Aequoria victoria* and its homologs have been cloned from various marine organisms. A number of optimized blue, cyan, and yellow mutants of GFP have also been developed (Shaner et al., 2005). While the cyan and yellow variants exhibit enhanced photochemical properties, existing blue fluorescent protein (BFP) variants are characterized by moderate intrinsic brightness (defined as the product of extinction coefficient and quantum yield) and low photostability. Recently, two improved BFP variants, Azurite and EBFP2, were introduced (Mena et al., 2006; Ai et al., 2007). Both Azurite and EBFP2 exhibited significant improvement in photostability compared with original BFP (GFP with Y66H/Y145F substitutions) and EBFP (GFP with F64L/Y66H/Y145F/V163A substitutions). The 1.6-fold and 2-fold enhancement in the brightness were achieved in Azurite and EBFP2, respectively. However, the brightness still was 0.43 and 0.56 of that of widely used green fluorescent probes, such as TagGFP or EGFP (Shaner et al., 2005).

The improvement in the brightness was mainly due to the increase in the quantum yields, but not in the molar extinction coefficients. Because all BFPs have His66 in the chromophore, we speculated that their low absorbance would be attributed to this residue, and its change to Tyr66, which is typically observed in green and yellow variants, such as EGFP and EYFP, could increase the extinction coefficient. However, earlier attempts to design BFP variant with Tyr66 in a protonated state on the basis of GFPs by blocking an excited-state proton transfer (ESPT) pathway, and in this way preventing the GFP chromophore from deprotonation, had only limited success, such as in the case of mKalama1 (Ai et al., 2007) and mutants of PSCFP (Chudakov et al., 2004). In both cases, the mutants had brightness and/or photostability lower than that of EBFP2. Therefore, we turned our attention to red fluorescent proteins (RFPs) with anionic chromophores, where ESPT has not been observed (Hosoi et al., 2006; Remington, 2006). Previously, we have shown that the DsRed-like red chromophore is mainly formed from a blue protonated GFP-like chromophore as an intermediate (Verkhusha et al., 2004). The intermediate has been detected during the maturation of several tetrameric red-shifted proteins, such as DsRed, hsriCP, and asulCP. We speculated that the same red chromophore formation mechanism should be preserved in other RFPs. Here, we use a structure-based directed evolution in combination with random mutagenesis to develop monomeric BFPs on the basis of the RFPs of different genetic background, such as TagRFP, mCherry, HcRed1, M355NA, and mKeima.

RESULTS AND DISCUSSION

We selected several monomeric RFPs, such as TagRFP (Merzlyak et al., 2007), mCherry (Shaner et al., 2004), mKeima (Kogure et al., 2006), and tetrameric RFPs, such as HcRed1 (Fradkov et al., 2002) and M355NA (Bulina et al., 2003), to introduce site-specific mutations preventing maturation of the chromophore beyond the blue protonated intermediate, and also stabilizing it. Our primary choice of positions for amino acid substitutions was based on several crystal structures, including those for eqFP611 (Petersen et al., 2003), which shares 76% homology with TagRFP (Merzlyak et al., 2007) and has similar chromophore environment (Figure 1A), mCherry (Shu et al., 2006), HcRed

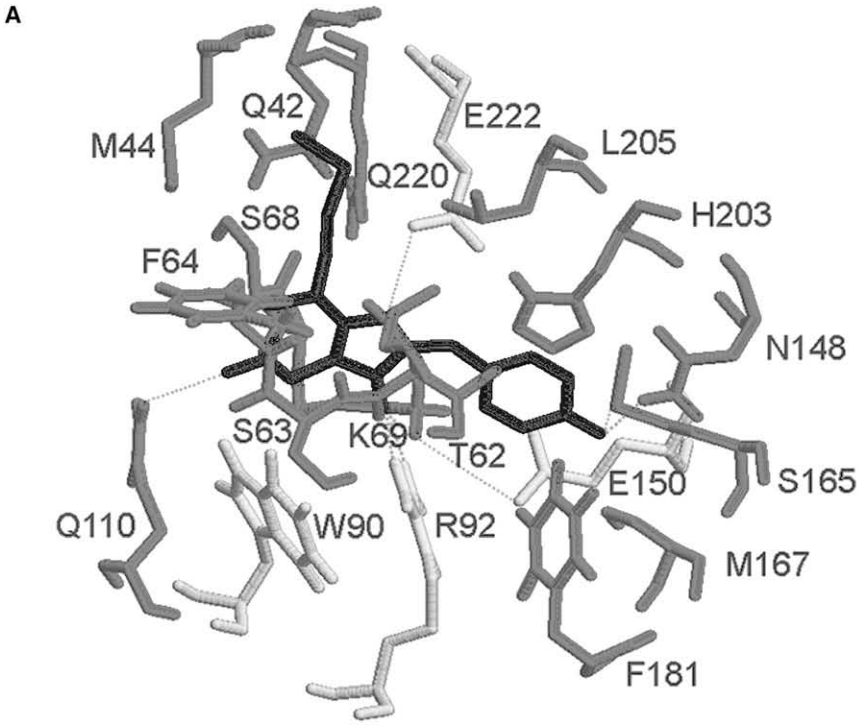

B

```
                10        20        30        40        50        60
EGFP        MVSKGEELFTGVVPILVELDGDVNGHKFSVSGEGEGDATY-GKLTLKFICTT-GKLPVPWPTL
Azurite      MSKGEELFTGVVPILVELDGDVNGHKFSVSGEGEGDATY-GKLTLKFICTT-GKLPVPWPTL
EBFP2       MVSKGEELFTGVVPILVELDGDVNGHKFSVRGEGEGDATN-GKLTLKFICTT-GKLPVPWPTL
eqFP611       MNSLIKENMRMMVVMEGSVNGYQFKCTGEGDGNP-YMGTQTMRIKVVEGGPLPFAFDIL
TagRFP      MSEELIKENMHMKLYMEGTVNNHHFKCTSEGEGKP-YEGTQTMRIKVVEGGPLPFAFDIL
mTagBFP     MSEELIKENMHMKLYMEGTVDNHHFKCTSEGEGKP-YEGTQTMRIKVVEGGPLPFAFDIL

                *** 70        80        90       100       110       120
EGFP        VTTFTYGVQCFSRYPDHMKQHDFFKSAMPEGYVQERTIFFKDDGNYKTRAEVKFEGDTLV
Azurite     VTTLSHGVQCFSRYPDHMKQHDFFKSAMPEGYVQERTIFFKDDGNYKTRAEVKFEGDTLV
EBFP2       VTTLSHGVQCFARYPDHMKQHDFFKSAMPEGYVQERTIFFKDDGTYKTRAEVKFEGDTLV
eqFP611     ATSFMYGSKTFIKHTKGIP--DFFKQSFPEGFTWERVTRYEDGGVFTVMQDTSLEDGCLV
TagRFP      ATSFMYGSRTFINHTQGIP--DFFKQSFPEGFTWERVTTYEDGGVLTATQDTSLQDGCLI
mTagBFP     ATSFTYGSKTFINHTQGIP--DFFKQSFPEGFTWERVTTYEDGGVLTATQDTSLQDGCLI

                130       140       150       160       170       180
EGFP        NRIELKGIDFKEDGNILGHKLEYNYNSHNVYIMADKQKNGIKVNFKIRHNIEDGSVQLAD
Azurite     NRIELKGIDFKEDGNILGHKLEYNFNSHNIYIMADKQKNGIKVNFKIRHNIEDGSVQLAD
EBFP2       NRIELKGVDFKEDGNILGHKLEYNFNSHNIYIMAVKQKNGIKVNFKIRHNVEDGSVQLAD
eqFP611     YHAKVTGVNFPSNGAVMQKKTKG-WEPNTEMLYPA--DGGLRGYSQMALNVDGGGYLSCS
TagRFP      YNVKIRGVNFPSNGPVMQKKTLG-WEANTEMLYPA--DGGLEGRSDMALKLVGGGHLICN
mTagBFP     YNVKIRGVNFTSNGPVMQKKTLG-WEATTETLYPA--DGGLEGRNDMALKLVGGSHLIAN

                190       200       210       220       230
EGFP        HYQQNTPIGD-GPVLLPDNHYLSTQSALSKDPNEKRDHMVLLEFVTAAGITHGMDELYK
Azurite     HYQQNTPIGD-GPVLLPDNHYLSTQSALSKDPNEKRDHMVLLEFRTAAGITHGMDELYK
EBFP2       HYQQNTPIGD-GPVLLPDSHYLSTQSVLSKDPNEKRDHMVLLEFRTAAGITLGMDELYK
eqFP611     FETTYRSKKTVENFKMPGFHFVDHRLERLEE-SDKEMFVVQHEHAVAKFCDLPSKLGRL
TagRFP      FKTTYRSKKPAKNLKMPGVYYVDHRLERIKE-ADKETYVEQHEVAVARYCDLPSKLGHKLN
mTagBFP     IKTTYRSKKPAKNLKMPGVYYVDYRLERIKE-ANNETYVEQHEVAVARYCDLPSKLGHKLN
```

Figure 1. Structural Basis of the Amino Acid Substitutions Converting TagRFP into the mTagBFP

(A) Immediate environment of the chromophore in eqFP611 (Petersen et al., 2003) that is highly homologous to TagRFP. The chromophore is showed in black, the conserved amino acid residues are in light gray, and nonconserved residues are in gray. The hydrogen bonds are indicated with dotted lines.

(B) Amino acid sequence alignment of mTagBFP with EGFP, Azurite, EBFP2, eqFP611, and TagRFP. Structurally important regions are highlighted in gray, α helices are shown with ribbons, and β strands are shown with arrows. The chromophore forming residues are marked with asterisks. Site-specific mutations resulted in conversion of TagRFP into a blue fluorescent predecessor of mTagBFP are shown white on black background. Mutations generated in the course of random mutagenesis are shown black italic on dark gray background. The alignment numbering follows that for EGFP.

(Wilmann et al., 2005), and KFP (Quillin et al., 2005) variant of asulCP, which is the precursor for M355NA.

In order to convert RFPs into BFPs, we first needed to stabilize the tyrosine-based chromophore in a protonated (neutral) state. In all known RFPs, position 65 (numbering is in accordance with EGFP alignment; see Figure 1B and Figure S1 available online) is occupied with Met, Gln, or Glu. We hypothesized that formation of a double acylamine bond specific for the red anionic chromophore would be less probable in the case of totally aliphatic or aromatic side chains, which could cause less polarization of the 65αC-H bond in the chromophore (Remington, 2006). Positions 148 and 165 are located in close proximity to the planar chromophores in RFPs. Side chains of the residues at positions 148 and/or 165 form hydrogen bonds with oxygen of the chromophore phenolate and, thus, stabilize the anionic form of the red chromophore. Substitutions at these positions could lead to prevention of the hydrogen bond formation with phenolate anion that can be favorable for formation of neutral blue chromophore. The side chain of the amino acid residue in position 181 forms van der Waals contacts with multiple amino acids, which are necessary for the formation and stabilization of the chromophore. In eqFP611 (Petersen et al., 2003), and in the suggested fluorescent state of KFP (Quillin et al., 2005), the hydroxyphenyl group of the red chromophore is coplanar with His203, and forms with it π-π interactions. It also develops the hydrogen bonds with Glu150 and Glu222. The latter is possibly involved in the catalytic process of the formation of DsRed-like chromophore (Yarbrough et al., 2001). In the mCherry and HcRed structures, position 203

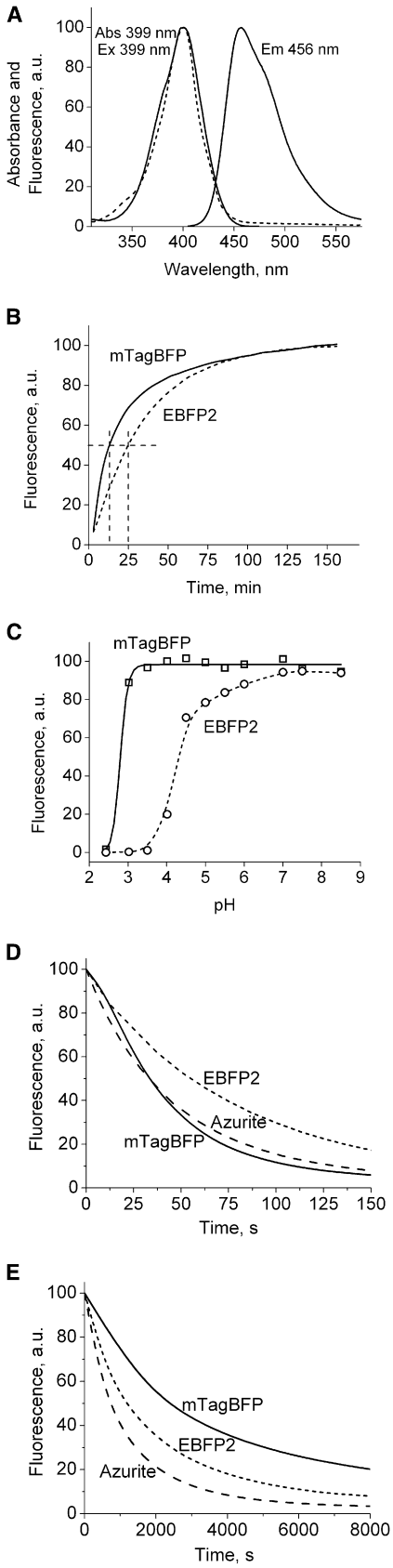

Figure 2. Spectral, Biochemical, and Photochemical Properties of the Purified mTagBFP

(A) Absorbance (dashed line), excitation, and emission spectra of mTagBFP.
(B) Maturation kinetics for mTagBFP and EBFP2.
(C) pH dependence for mTagBFP and EBFP2.
(D) Photobleaching curves for purified mTagBFP (solid line), EBFP2 (short dashed line), and Azurite (dashed line) under mercury arc lamp illumination.
(E) Photobleaching curves for mTagBFP (solid line), EBFP2 (short dashed line) or azurite (dashed line) expressed in HeLa cells using 405 nm laser scanning. Data represent an average of 8–10 cells per each protein. The time axes in (D) and (E) represent the normalized imaging time with an initial emission rate of 1000 photons/s/molecule.

is occupied with Ile, which contacts chromophore and its surrounding residues. Therefore substitutions at position 203 would simultaneously stabilize the neutral blue chromophore intermediate and possibly cause change in the hydrogen bonding with Glu222.

First, we tested our structure-based design to convert TagRFP into BFP. Based on the above analysis, we performed the site-specific saturated mutagenesis of Met65, Asn148, Ser165, Phe181, and His203 residues of TagRFP by the overlap extension approach (Ho et al., 1989). The bacterial library consisting of about 3×10^7 independent clones (theoretical size was 3×10^6) has been screened with the fluorescence-activated cell sorter (FACS) followed by selection of the best clones on Petri dishes using fluorescence stereomicroscope. The screening has identified several blue mutants with a blue emission when excited either with 407 nm krypton laser line on FACS or with 390/40 nm filter. Compared to TagRFP the mutants had M65L,H,F/N148F,I,W/S165N,I,A,T/F181I,A,V/H203Y,F substitutions. In order to increase the brightness and photostability, we next used the mixture of the mutants to perform several rounds of random mutagenesis by an error-prone polymerase chain reaction (PCR). Bacterial libraries of 5×10^6 to 2×10^7 clones were applied to the high-throughput screening by FACS. After each round, the 20–50 brightest blue clones with minimal green and red fluorescence were analyzed by sequencing, and mixture of several of the best variants were then used as a template for the next round of mutagenesis. If, during screening, the external mutations at the β can-dimerizing interfaces were observed, such as V106M, T108I, R126I, and K182N (Merzlyak et al., 2007), they were reversed by site-specific mutagenesis. After five sequential rounds of random mutagenesis and FACS screening, an enhanced bright blue mutant, mTagBFP, with an additional eight amino acid substitutions, was found. Among them, R69K/C179A were internal, and N23D/P131T/M151T/G175S/D213N/K214N were external to the β can (Figure 1B). The mTagBFP exhibited the excitation/emission peaks at 399/456 nm, respectively (Figure 2A and Table 1).

Next, we performed the multiple site-specific mutagenesis of mCherry, HcRed1, M355NA, and mKeima. Because, during the screening of TagRFP libraries, we observed its blue variants with 69R,K and 84W,L,F residues, we added these two positions to positions 65, 148, 165, 181, and 203, suggested on the basis of the protein structures. The semirandom mutagenesis at the seven positions resulted in several blue variants for each of mCherry, HcRed1, M355NA, and mKeima proteins. These variants contained: M65L,F/K69R,K/L84W,L/S148F,I/I165V,I,

Table 1. Properties of mTagBFP in Comparison with BFPs Containing a Histidine in the Chromophore

Protein	Excitation Maximum (nm)	Emission Maximum (nm)	Extinction Coefficient (M^{-1} cm^{-1})	Quantum Yield	Brightness Relative to EBFP2	Effective pK_a	Fluorescence Lifetime (ns)	Maturation Half-Time (min)	$t_{1/2}$ Bleach (Arc Lamp) (s)	$t_{1/2}$ Bleach (Confocal) (s)
EBFP	383	445	27,100[a]	0.34[a]	0.51	6.3[b]	n.d.[c]	n.d.	n.d.	n.d.
Azurite	383	447	26,200[a]	0.55[a]	0.80	5.0[b]	3.4 ± 0.2	18 ± 2	33	710
EBFP2	383	448	32,000[b]	0.56[b]	1.00	4.5 ± 0.2	3.0 ± 0.2	25 ± 2	55	1,140
mTagBFP	399	456	52,000 ± 500	0.63 ± 0.02	1.82	2.7 ± 0.2	2.6 ± 0.1	13 ± 2	34	2,380

Error terms presented are SEM.
[a] Data are from Mena et al. (2006).
[b] Data are from Ai et al. (2007).
[c] n.d., not determined.

T/V181A,V/I203Y substitutions in the case of mCherry, E65H,F/R69K,R/F84W/S148F,I/N165A,V,N/H181A,T/I203Y,F in the case of HcRed1, M65H/K69K/F84F/S148F/S165A,V/L181I,V,T/H203F in the case of M355NA, and Q65H/I69K,R/F84W/S148I,F/D165A,V,T/F181A,V,T/R203Y,F in the case of mKeima. The observed mutations were very similar to those found in the TagRFP site-specific blue variants. The purified recombinant mutant proteins had excitation/emission peaks at 399–410/450–461 nm. The best blue variants, named mCherry-Blue, HcRed1-Blue, M355NA-Blue, and mKeima-Blue, have mutations and spectroscopic properties summarized in Table 2 and Figure S1. Based on the analogous results obtained for five RFPs of the different genetic background, we concluded that introduction of 65L,H/69K/84F,W,L/148F,I/165A,I,N/181A,I/203F,Y mutations into other RFPs with the tyrosine-based chromophore most likely would convert them into blue variants. Screening of these mutant libraries should be easy, because a number of the distinctive mutants in each library will be limited to 144.

The amino acid substitutions that resulted in the formation of the BFPs are in good agreement with our predictions based on the respective structures of the RFPs (Yarbrough et al., 2001; Petersen et al., 2003; Quillin et al., 2005; Wilmann et al., 2005; Shu et al., 2006). First, there are totally aliphatic or aromatic side chains of Leu/His in position 65 in BFPs. Second, there is Lys69 in combination with the hydrophobic amino acid in position 84. Third, the hydrophobic Phe and Ile in position 148, and aliphatic side chain of Ala/Ile in position 165, are not able to form hydrogen bonds with phenolate anion of the chromophore. The amide group of Asn165 in mTagBFP is a weaker hydrogen bond donor than the hydroxyl of Ser in TagRFP and eqFP611. Fourth, there are aromatic side chains of Tyr/Phe in position 203, and aliphatic Ala/Ile in position 181. These substitutions promote the formation and stabilization of the tyrosine-based neutral chromophore.

We further studied properties of our advanced monomeric mTagBFP and compared it with EBFP2, which is probably the best monomeric BFP reported to date (Ai et al., 2007). The mTagBFP exhibited monomeric behavior at 10 mg/ml in vitro and, when expressed as a fusion tag with polymerizing proteins, such as β actin and α tubulin in mammalian cells (Figure S2), that was similar to the parental TagRFP (Merzlyak et al., 2007). Compared to EBFP2, mTagBFP is characterized by 1.6-fold-higher molar extinction coefficient and the higher quantum yield (Table 1 and Figure S3), which results in more than a 1.8-fold brighter fluorescence. These characteristics make an intrinsic brightness of mTagBFP similar to that of commonly used EGFP (Patterson et al., 2001; Shaner et al., 2005). Maturation half-time for mTagBFP at 37°C is twice as short as that for EBFP2, and pH stability of mTagBFP is much better (pK_a is below 3.0) (Figures 2B and 2C). Among other mutations, we presume that P131T substitution plays a key role in accelerating mTagBFP folding and/or maturation, as it has been shown for a superglo-GFP (Flores-Ramírez et al., 2007).

In order to test photostability of mTagBFP in comparison with the most photostable, available BFPs, such as Azurite and EBFP2, we performed photobleaching experiments both in aqueous drops of the purified proteins in oil with an epifluorescence microscope equipped with a 100 W mercury arc lamp source and DAPI 350/50 filter, and in HeLa cells with a 405 nm laser confocal microscope. Photostability of fluorescence probes can be compared on the basis of a half-time for the decrease of the initial photon emission rates. In the standard photobleaching procedure (Shaner et al., 2005), the photobleaching half-time for both mTagBFP and Azurite was about 0.6 of that

Table 2. Properties of the Blue Mutants of mCherry, HcRed1, M355NA, and mKeima

RFP	Peak (nm)		Position[a]							Peak after Mutagenesis (nm)	
	Excitation	Emission	65	69	84	148	165	181	203	Excitation	Emission
mCherry	587	610	L	K	L	F	I	A	Y	403	458
HcRed1[b]	588	618	H	K	W	I	A	A	Y	408	455
M355NA[c]	576	592	H	K	F	F	A	I	F	409	461
mKeima	440	620	H	K	W	I	A	A	Y	399	451

[a] Amino acid substitutions at the indicated positions resulted in the brightest blue mutants.
[b] HcRed1 data are from Fradkov et al. (2002); a commercial protein, HcRed1 (Clontech), is the HcRed2A protein originally reported by Gurskaya et al. (2001).
[c] M355NA (Bulina et al., 2003) is the nonaggregating variant of the commercial AsRed2 protein (Clontech).

for EBFP2 (Figure 2D and Table 1). With this approach, the photostabilities of other FPs, such as cyan mCerulean or yellow mVenus, are similar to that of mTagBFP (Shaner et al., 2007). However, the photostability of mTagBFP under laser scanning confocal illumination was 2.1-fold and 3.3-fold higher than that for EBFP2 and Azurite, respectively (Figure 2E). The difference in the photostabilities measured under a continuous light source, such as arc lamp, and a periodic source, such as scanning laser, have been described previously (Shaner et al., 2008). It may reflect two distinctive regimes of the light illumination, in which the former does not, but the latter does allow the chromophore to remain for a relatively long time in a ground state before the next cycle of the excitation and photon emission.

Fluorescence lifetimes for mTagBFP, EBFP2, and Azurite were measured under several conditions. The measured, time-resolved fluorescence intensity decays of all these proteins were monoexponential. At pH 7.4 and 23°C, the fluorescence lifetimes of mTagBFP, EBFP2, and Azurite were 2.6, 3.0, and 3.4 ns, respectively (Table 1). The pH change from 7.4 to 6.0 did not change the lifetime for mTagBFP, but decreased lifetime for Azurite and increased lifetime for EBFP2 (Figure 3). The temperature increase from 23°C to 37°C resulted in the decrease of all fluorescence lifetimes. At tested conditions, mTagBFP exhibited the shortest lifetime among available BFPs, making it a distinctive lifetime probe for monochromatic lifetime imaging.

The emission spectrum of mTagBFP and absorbance spectra of GFPs exhibited substantial overlap, suggesting that mTagBFP can be a good donor for GFP acceptor in Förster resonance energy transfer (FRET). Among available GFPs, TagGFP was chosen because of the low absorbance below 400 nm, where mTagBFP is excited. Construction of the FRET indicators, based on fluorescent proteins, principally requires that the donor and acceptor are monomeric. Introduction of the well-known monomerizing mutation A206K into TagGFP has resulted in a slight decrease in its brightness. In order to rescue the brightness and to increase the molar extinction coefficient, we performed saturated site-specific mutagenesis at positions 99, 153, and 163. It has been shown that a mutant of EGFP, called folding-reporter GFP (Crameri et al., 1996), with substitutions F99S/M153T/V163A, has a molar extinction coefficient 1.5-fold higher than that for EGFP (Pedelacq et al., 2006). Indeed, our screening has identified the bright mutant of TagGFP/A206K with L99Q/M153R/V163A mutations, named mTagGFP (Figure S4). The mTagGFP has the excitation/emission peaks of 483/506 nm (Figure S5). Comparison of the purified proteins revealed that mTagGFP has a slightly higher molar extinction coefficient and quantum yield compared with parental TagGFP and EGFP (Table S1). The introduced mutations did not affect mTagGFP pH stability (pK_a = 5.0), which is higher than that of EGFP, but resulted in 1.6-fold-faster maturation compared with TagGFP (Figure S6).

To estimate the potential efficiency of FRET between mTagBFP or EBFP2 as donors, and mTagGFP as an acceptor, we calculated the Förster distances, R_0, for the donor-acceptor pairs, as has been described previously (Galperin et al., 2004). The calculation yielded values of R_0 = 5.25 nm for mTagBFP-mTagGFP and R_0 = 5.13 nm for EBFP2-mTagGFP, suggesting that the former pair is a better FRET pair. Both Förster distances were larger than those reported for the standard ECFP-EYFP and mCyPet-mYPet pairs (Table 3). We then constructed and

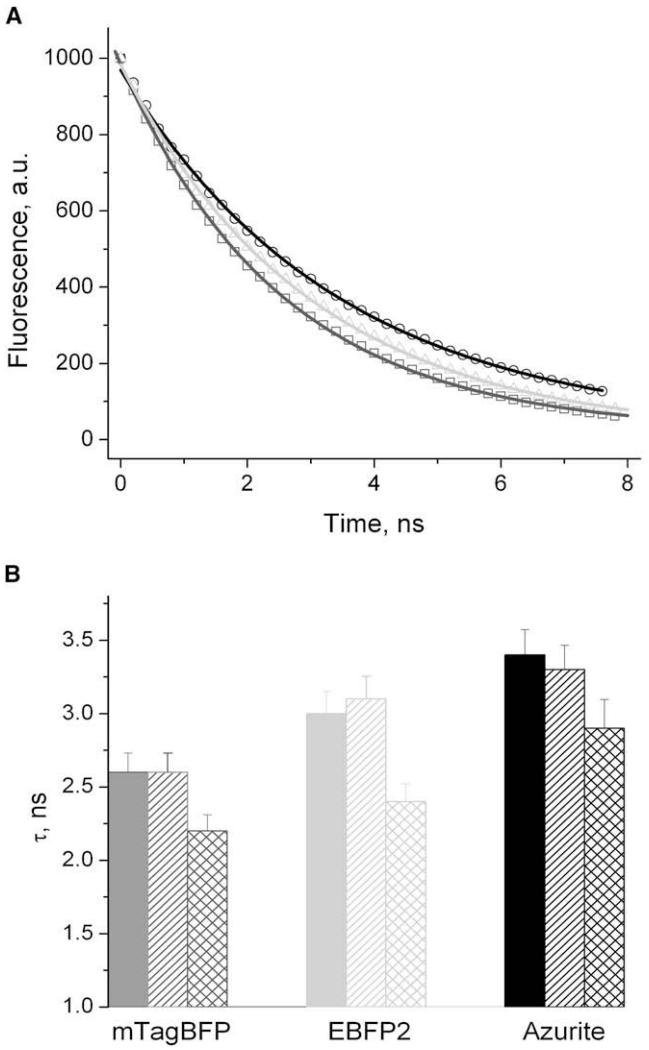

Figure 3. Fluorescence Lifetimes for the Purified mTagBFP, EBFP2 and Azurite

(A) Fluorescence decay for mTagBFP (dark gray squares), EBFP2 (light gray triangles) and Azurite (black circles) at pH 7.4 and 23°C. Solid lines indicate fits by the mono-exponential curves.

(B) Dependence of fluorescence lifetimes for mTagBFP (dark gray), EBFP2 (light gray), and Azurite (black) on pH value and temperature: pH 7.4 at 23°C (filled bars); pH 6.0 at 23°C (diagonal bars); pH 7.4 at 37°C (diamond bars). Error bars represent SEM, and do not exceed 5%.

purified fusion proteins consisting of a tandem of either mTagBFP and mTagGFP or EBFP2 and mTagGFP, each containing the caspase-3 cleavage sequence, DEVD, within the linker between fluorescent proteins. Emission spectra were measured before and after digestion with trypsin. Cleavage of the fusion proteins led to a decrease in green emission of mTagGFP acceptor and a simultaneous increase in blue emission of mTagBFP (Figure 4A) and EBFP2 (Figure S7) donors due to elimination of FRET similar to what has been observed with fusion constructs of other fluorescent proteins. Calculation of FRET efficiencies, E, based on the increase of donor emission upon cleavage of the fusion proteins produced E = 0.57 for mTagBFP-mTagGFP and E = 0.38 for EBFP2-mTagGFP pairs,

Table 3. FRET Characteristics for Several Fusion Constructs of the Fluorescent Proteins

Fusion Construct	R_0 (nm)	E	Reference
mTagBFP-mTagGFP	5.25	0.57 ± 0.03	This article
EBFP2-mTagGFP	5.13	0.38 ± 0.03	This article
ECFP-EYFP[a]	4.86	0.42[b]	(Galperin et al., 2004; Patterson et al., 2000)
mCyPet-mYPet[c]	4.93[d]	0.51[b]	(Nguyen and Daugherty, 2005; Ohashi et al., 2007)

The Förster distances (R_0) were calculated under the standard assumption of the random orientation of the chromophores. The FRET efficiencies (E) were experimentally measured using the physically linked donor and acceptor proteins. Error terms presented are SEM.

[a] Proteins of this widely used standard FRET pair have a tendency to form the dimer. Data on monomerized versions of the proteins are not available.

[b] The ECFP-EYFP pair has nine amino acid linker (Galperin et al., 2004). The mCyPet-mYPet pair has 12 amino acid linker (Ohashi et al., 2007).

[c] Monomerized versions of CyPet and YPet proteins, which have been specifically optimized for FRET through multiple rounds of site-specific and random mutagenesis (Ohashi et al., 2007). It was shown, though, that the original CyPet and YPet proteins form hetero- and homodimers in solution substantially enhanced the observed FRET efficiency.

[d] Calculated from the data of Nguyen and Daugherty (2005).

respectively. For comparison, FRET efficiencies reported for ECFP-EYFP and mCyPet-mYPet pairs were 0.42 and 0.51, respectively (Table 3). These data suggest that the mTagBFP-mTagGFP pair is not only superior to other BFP-GFP pairs, but is one of the best among available FRET pairs of the true monomeric fluorescent proteins.

In order to explore the benefits of the large Förster distance and enhanced FRET efficiency exhibited by the purified mTagBFP-mTagGFP pair, we applied it to detect apoptosis in living HeLa cells. We used the two-filter method of sensitized FRET measurements (Gordon et al., 1998) on a pixel-by-pixel basis, as described in our previous study (Galperin et al., 2004). The initial mean FRET efficiency in vivo normalized to donor fluorescence was 51.5%. Following 40–80 min exposure to 1 μM staurosporine, the FRET gradually dropped to zero before the shrinking of cells characteristic to apoptosis (Figures 4B and 4C). The large FRET efficiency of the mTagBFP-mTagGFP pair enabled the detection of even weak proteolitic activity in each cell at the beginning of apoptosis, when only a fraction of the substrate was cleaved. When mTagBFP and mTagGFP free proteins were coexpressed in HeLa cells, the cross-bleed-corrected FRET normalized to fluorescence of donor was 0.85%. Under our experimental conditions, we observed that FRET between ECFP and EYFP free proteins coexpressed in HeLa cells was 6.2%, confirming their weak dimerizing tendency. It has been shown that the ECFP-EYFP pair linked with a 19 amino acid peptide provided 48% of the FRET efficiency in HeLa cells (Domingo et al., 2007). The same authors documented 5% FRET efficiency between ECFP and EYFP coexpressed free proteins, which is consistent with our data. Thus, the mTagBFP and mTagGFP proteins derived from the different marine sources and, as a result, lacking ability to form heterodimers, provide more than 6-fold-lower background for FRET analysis than the weakly dimerizing FRET pairs, such as the ECFP-EYFP.

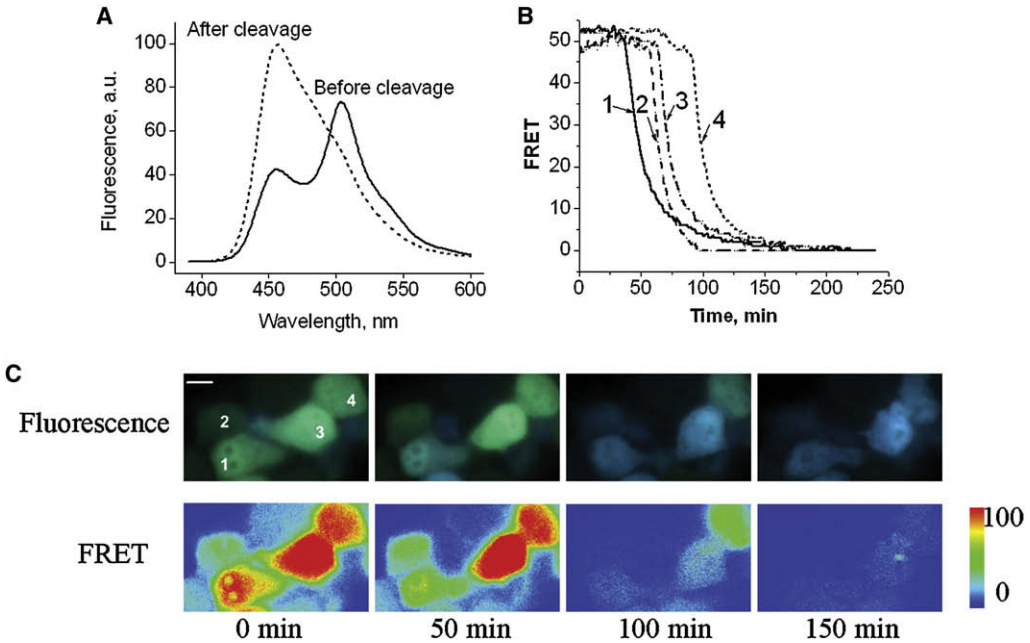

Figure 4. Behavior of the mTagBFP as the FRET Donor

(A) FRET of mTagBFP-mTagGFP fusion construct in vitro.

(B and C) Imaging of FRET intensity in staurosporine-treated HeLa cells: (B) time course of corrected FRET normalized per donor fluorescence observed in four cells indicated in (C). The values are normalized to time of the staurosporine addition. (C) Fluorescent images of the cells after staurosporine treatment are shown as overlaid images of blue and green channels in upper panels. The corrected FRET signals are shown as pseudocolor images in lower panels. Scale bar, 10 μm.

SIGNIFICANCE

We developed the structure-based directed evolution approach allowing conversion of red fluorescent proteins (RFPs) into blue fluorescent proteins (BFPs) with a tyrosine chromophore. Among five different BFP variants obtained by this strategy, enhanced mTagBFP protein has the intrinsic brightness similar to that of EGFP. An almost 2-fold increase in brightness of mTagBFP compared with available BFPs with the histidine residue allows the use of twice-less intensities of excitation light and, consequently, will harm mammalian cells and tissues less, while allowing the acquisition of images with better signal-to-noise ratio. The higher pH-stability makes mTagBFP suitable for visualization in acidic compartments, and increases reliability of FRET-based and protein translocation assays. The less-structured and narrower fluorescence emission spectrum of mTagBFP compared with EBFP2 (semi-widths for the spectra are 59 and 70 nm, respectively) provides for more accurate spectral separation with other fluorescent probes that makes it an advantageous tag for multicolor labeling. The spectral characteristics of mTagBFP would allow for simultaneous use of two FRET pairs in a single cell: the first consisting of blue-green, and the second consisting of orange-red FPs. The faster mTagBFP maturation will be advantageous to study promoter activities and early stages of protein expression. Altogether, these properties make mTagBFP the protein of choice for cell and tissue imaging in the blue part of the visible spectrum. mTagBFP will also be useful for in vivo applications, such as in transgenic animal models to study neurodegenerative diseases and cancer (Hoffman, 2008).

EXPERIMENTAL PROCEDURES

Mutagenesis and Library Screening

TagRFP (Merzlyak et al., 2007), mCherry (Shaner et al., 2004), mKeima (Kogure et al., 2006), HcRed1 (Fradkov et al., 2002), and M355NA (Bulina et al., 2003) were PCR amplified as BglII-EcoRI fragment and inserted into pBAD/His-B vector (Invitrogen). Site-specific mutagenesis was performed with the QuickChange Mutagensis Kit (Stratagene). For simultaneous mutagenesis at several positions, including a site-specific saturated mutagenesis (i.e., all 20 amino acids were encoded with the mixture of primers), the overlap-extension approach was applied (Ho et al., 1989). Random mutagenesis was performed with GeneMorph II Random Mutagenesis Kit (Stratagene) under conditions resulting in mutation frequency of up to 16 mutations per 1000 base pairs. After mutagenesis, a mixture of the mutants was electroporated into LMG194 host cells (Invitrogen).

Typical mutant libraries for each FACS screen consisted of about 10^6–10^7 independent clones. Protein expression in the libraries was induced overnight at 37°C with 0.002% arabinose. The next morning, the expressing bacteria were washed with phosphate buffered saline (PBS) and then diluted with PBS for FACS sorting to an optical density of 0.02 at 600 nm. MoFlo cell sorter (Dako) equipped with standard argon, krypton, and argon-krypton mixed-gas lasers was used. Typically, about 10 sizes of each library were sorted on the FACS with 407 nm of krypton excitation line and 450/65 nm emission filter. The collected bright blue bacterial cells were rescued in rich SOC medium at 37°C for several hours, and then plated on Petri dishes with 0.02% arabinose. The next day, the dishes were analyzed with a Leica MZ16F fluorescence stereomicroscope with a custom blue filter set (390/40 nm exciter, 460/40 nm emitter) from Chroma. For further analysis, the 20–50 brightest clones were selected and applied for sequencing. A mixture of several of the best variants was then used as a template for the next round of random mutagenesis.

Protein Characterization

Recombinant proteins with polyhistidine tags were expressed in LMG194 bacterial cells grown overnight in RM minimal medium supplemented with 0.002% arabinose and then purified with Ni-NTA agarose (QIAGEN). The excitation and emission spectra were measured with the FluoroMax-3 spectrofluorometer (Jobin Yvon). For absorbance measurements, the Hitachi U-2000 spectrophotometer was used.

In order to study protein maturation, LMG194 bacterial cells were grown at 37°C overnight in RM minimal medium supplemented with ampicillin. The next morning, cells were diluted to an optical density of 1.0 at 600 nm, and 0.2% arabinose was added. Upon induction of protein expression, the bacterial cultures were grown at 37°C in 50 ml tubes filled to the brim and tightly sealed to restrict oxygen availability. After 1 hour the cultures were centrifuged in the same tightly closed tubes. After opening the tubes, the proteins were purified with Ni-NTA resin within 30–40 min with all procedures and buffers at or below 4°C. Protein maturation was performed at 37°C in 50 mM NaH_2PO_4, 300 mM NaCl, 5 mM mercaptoethanol, pH 8.0, with the FluoroMax-3 spectrofluorometer.

In order to determine extinction coefficients, we relied on measuring of mature chromophore concentrations, for which the purified proteins were either acid or alkali denatured. It is known that extinction coefficient of the synthetic compound of the tyrosine-containing GFP-like chromophores is 44,000 M^{-1} cm^{-1} at 447 nm in 1 M NaOH (Chudakov et al., 2004), and about 28,500 M^{-1} cm^{-1} at 382 nm in 1 M HCl (Niwa et al., 1996). Based on the absorbance of the native and denatured proteins, molar extinction coefficients for the native states were calculated.

For determination of the quantum yields, the fluorescence of the blue and green mutant variants was compared with equally absorbing EBFP2 (quantum yield, 0.56 [Ai et al., 2007]) and EGFP (quantum yield, is 0.60 [Patterson et al., 2001]), respectively. pH titrations were performed with a series of buffers (100 mM NaOAc, 300 mM NaCl for pH 2.5–5.0, and 100 mM NaH_2PO_4, 300 mM NaCl for pH 4.5–9.0).

Photobleaching measurements with purified proteins were performed with microdroplets of freshly purified proteins at 0.7 mg/ml in PBS under mineral oil in a chamber on the stage of an Olympus IX81 inverted microscope equipped with a 100 W mercury arc light source, 60× oil immersion lens and standard DAPI 350/50 excitation filter (Chroma). Single drops were found at low light levels (0.15% ND filters). ND filters were then removed, and the protein drops were photobleached. Photobleaching experiments have been performed under identical conditions for mTagBFP, EBFP2, and Azurite. The time to photobleach from 1000 down to 500 emitted photons per second was calculated according to the standard procedure of measuring photostability of fluorescent proteins (Shaner et al., 2005). In brief, for epifluorescence sources, such as arc lamp, the procedure took into account the spectral output of the source, transmission profile of excitation filter and dichroic mirror, absorbance spectra of the BFPs, and their quantum yields. EBFP2, which has been characterized according to this procedure in the original article (Ai et al., 2007), was used as the reference.

Fluorescence lifetime measurements were performed on an IX71 Olympus microscope with a 60× oil immersion lens equipped with a PicoStar (LaVision, Germany) time-gated camera and a Chameleon Ultra Titanium-Sapphire laser (Coherent) with an 80 MHz repetition rate tuned to 798 nm output. The TTL signal of the laser was used to synchronize the delay generator of the PicoStar system. Using an ultrafast harmonic generation system (Coherent), the second harmonic of the fundamental beam was generated and separated by a dichroic long-pass filter. The beam width of the resulting beam, with a wavelength of 399 nm, was adjusted with a 12.5× telescope to provide even illumination of the sample, and intensity was regulated with an ND filter. Laser scattering and background signal was removed from the emission signal with a 447/60 band pass filter (Semrock), and the remaining signal passed onto the time-gated CCD intensifier of the PicoStar system. Data were acquired with 6–8 mW laser power in front of the telescope. An objective heater and a heated stage inset (Bioptechs) were used for experiments at 37°C. The 30 μl protein samples at a concentration of 0.1 mg/ml were allowed to equilibrate for at least 10 min prior to data acquisition.

FRET Analysis

The mTagBFP-mTagGFP and EBFP2-mTagGFP fusion constructs containing N-terminal Strep tag (amino acids -WSHPQFEK-) and C-terminal polyhistidine

tag were cloned as NcoI-XbaI fragments into pBAD/Myc-His B vector (Invitrogen). The fusions contained the 20 amino acid linker -EFGGSGSDEVD KLGGSGSGT- with the caspase-3 recognition site (underlined). After overnight expression in LMG194 bacterial cells at 37°C, the constructs were isolated with Ni-NTA agarose (QIAGEN) followed by additional purification with Strep-Tactin sepharose (IBA). The purified constructs, at concentrations of 100 μg/ml, were digested with 30 μg/ml of trypsin for 2 hr at 37°C.

The Förster distances, R_0, were calculated as previously described (Galperin et al., 2004). In brief, when donor is excited, the nearby acceptor can receive energy from the donor with efficiency, E, expressed as: $E = R_0^6/(R_0^6 + r^6)$ (Lakowicz, 1999), where R_0 is defined by the equation $R_0^6 = (8.785 \times 10^{17}) \times \Phi \times \kappa^2 \times n^{-4} \times J(\Phi,\varepsilon,\lambda)^6$, where Φ is a quantum yield of the donor, κ^2 is the orientation factor for dipole coupling, n is the refractive index of the media, $J(\Phi,\varepsilon,\lambda)$ is the overlap integral of the emission spectrum of the donor and the absorption spectrum of the acceptor. We calculated Förster distances for the pairs of fluorescent proteins with Origin software (Microcal) with the values for the refraction index of water at 25°C, n = 1.334. The orientation factor for dipole coupling κ^2 is a relative orientation factor between the interacting dipoles. Under the standard assumption of the random orientation of chromophores in the interacting pairs, it has a value of 2/3. The FRET efficiency, E, for each pair of fluorescent proteins was experimentally measured from an increase in the donor fluorescence resulting from separation of the donor and acceptor after cleavage of the fusion construct.

Mammalian Plasmid Construction

In order to construct pmTagBFP-C1 and pmTagGFP-C1 plasmids, mTagBFP and mTagGFP were PCR amplified as NheI-BglII fragments and swapped with EGFP gene in pEGFP-C1 vector (Clontech). In order to construct pmTagBFP-N1 and pmTagGFP-N1 plasmids, mTagBFP and mTagGFP were PCR amplified as AgeI-NotI fragments and swapped with EGFP gene in pEGFP-N1 vector (Clontech) (the pEBFP2-C1 and pEBFP2-N1 plasmids were generous gifts of R. Campbell and M. Davidson; the pazurite-C1 and pazurite-N1 plasmids were kind gifts of P. Daugherty and M. Davidson).

In order to generate mTagBFP-α-tubulin fusion protein, a PCR-amplified NheI/BglII fragment encoding mTagBFP was swapped with TagGFP gene in pTagGFP-α-tubulin vector (Evrogen, Russia). In order to generate mTagBFP-β-actin fusion protein, a PCR-amplified AgeI/BglII fragment encoding mTagBFP was swapped with TagGFP in pTagGFP-β-actin vector (Evrogen, Russia). For FRET in mammalian cells, mTagBFP-mTagGFP fusion containing the 20 amino acid linker -EFGGSGSDEVDKLGGSGSGT- was PCR amplified as AgeI-NotI fragment and swapped with EGFP gene in pEGFP-N1 vector (Clontech).

Mammalian Cell Imaging

HeLa cells were grown on 23 mm glass-bottom dishes (Bioptechs) in minimum essential medium (Invitrogen) supplemented with 10% fetal bovine serum (HyClone). Transfection was performed with Lipofectamine-2000 (Invitrogen).

For imaging of mTagBFP-β-actin and mTagBFP-α-tubulin fusion constructs in mammalian cells, a Leica AFLX 6000 inverted fluorescence microscope equipped with a 63× glycerol objective lens was used. For photobleaching experiments with mTagBFP, Azurite and EBFP2 cytoplasmically expressed in mammalian cells, a Zeiss LSM 510 META DuoScan microscope, equipped with a 50 mW 405 nm laser, 460/40 nm emitter, and 63× oil objective lens, was used. Imaging at the beginning and after every bleaching step was performed with a maximal pinhole, 1% power of a 405 nm laser, 512 × 512 resolution, zoom 1, gain 500, and scan speed 1.61 μs/pixel, which corresponds to 0.986 s/frame. Each bleaching step was performed at 40% laser power and the same scan speed. Calculation of times to photobleach from an initial scan-averaged rate of 1000 emitted photons/s to 500 photons/s was performed essentially as has been described previously (Shaner et al., 2008). In brief, the procedure took into account the output power of the laser, energy of photons, scanned area, extinction coefficients of the BFPs at the laser wavelength, and their quantum yields.

For apoptosis analysis, cells 24 hr after transfection were treated with 1 μM staurosporine (Sigma-Aldrich) in a medium buffered with HEPES (20 mM, pH 7.2). Cells were then covered with mineral oil, placed onto a DeltaT microscopic stage heating unit (Bioptechs) at 37°C, and subjected to fluorescence imaging. The imaging workstation consisted of the Olympus IX81 inverted microscope equipped with a 60× oil immersion lens, cooled ORCA-AG camera (Hamamatsu), dual filter wheels, and Xenon arc light source, all controlled with SlideBook 4.1 software (Intelligent Imaging Innovation). Filter sets for image capture consisted of the standard filters from Chroma 74673 (403/12 nm exciter), 66974 (457/50 nm emitter), and 86100 dichroic mirror. After calibration for cross-bleed coefficients, the corrected FRET was calculated on a pixel-by-pixel basis with the FRET option of SlideBook 4.1 software. The details of the calculation procedures have been previously described (Gordon et al., 1998; Galperin et al., 2004).

SUPPLEMENTAL DATA

Supplemental Data include seven figures, one table, and a Supplemental Reference and can be found with this article online at http://www.chembiol.com/cgi/content/full/15/10/1116/DC1/.

ACKNOWLEDGMENTS

We thank R. Campbell, P. Daugherty, and M. Davidson for the plasmids with EBFP2 and Azurite genes. We are grateful to W. King for the assistance with flow cytometry. This work was supported by National Institutes of Health grants GM070358 and GM073913 (to V.V.V.) and AA013148 (to M.Y.). Additional support was provided by grants EC FP-6 Integrated Project LSHG-CT-2003-503259 and NATO Collaborative Linkage grant CBP.NR.NRCLG 981752. D.M.C. was supported by grants from the President of the Russian Federation and Rosnauka 02.512.11.2216. D.G. was supported by postdoctoral fellowship GR3388/1 from the Deutsche Forschungsgemeinschaft. The Einstein Flow Cytometry Core Facility was supported by a Cancer Center grant from NCI (CA13330) and by a Center for AIDS Research grant from NIAID (AI051519).

Received: January 28, 2008
Revised: July 2, 2008
Accepted: August 4, 2008
Published: October 17, 2008

REFERENCES

Ai, H.W., Shaner, N.C., Cheng, Z., Tsien, R.Y., and Campbell, R.E. (2007). Exploration of new chromophore structures leads to the identification of improved blue fluorescent proteins. Biochemistry *46*, 5904–5910.

Bulina, M.E., Verkhusha, V.V., Staroverov, D.B., Chudakov, D.M., and Lukyanov, K.A. (2003). Hetero-oligomeric tagging diminishes non-specific aggregation of target proteins fused with *Anthozoa* fluorescent proteins. Biochem. J. *371*, 109–114.

Chudakov, D.M., Verkhusha, V.V., Staroverov, D.B., Lukyanov, S., and Lukyanov, K.A. (2004). Photoswitchable cyan fluorescent protein for protein tracking. Nat. Biotechnol. *22*, 1435–1439.

Crameri, A., Whitehorn, E.A., Tate, E., and Stemmer, W.P. (1996). Improved green fluorescent protein by molecular evolution using DNA shuffling. Nat. Biotechnol. *14*, 315–319.

Domingo, B., Sabariegos, R., Picazo, F., and Llopis, J. (2007). Imaging FRET standards by steady-state fluorescence and lifetime methods. Microsc. Res. Tech. *70*, 1010–1021.

Flores-Ramírez, G., Rivera, M., Morales-Pablos, A., Osuna, J., Soberón, X., and Gaytán, P. (2007). The effect of amino acid deletions and substitutions in the longest loop of GFP. BMC Chem. Biol. *7*, 1. 10.1186/1472-6769-7-1.

Fradkov, A.F., Verkhusha, V.V., Staroverov, D.B., Bulina, M.E., Yanushevich, Y.G., Martynov, V.I., Lukyanov, S., and Lukyanov, K.A. (2002). Far-red fluorescent tag for protein labeling. Biochem. J. *368*, 17–21.

Galperin, E., Verkhusha, V.V., and Sorkin, A. (2004). Three-chromophore FRET microscopy to analyze multiprotein interactions in living cells. Nat. Methods *1*, 209–217.

Gordon, G.W., Berry, G., Liang, X.H., Levine, B., and Herman, B. (1998). Quantitative fluorescence resonance energy transfer measurements using fluorescence microscopy. Biophys. J. *74*, 2702–2713.

Gurskaya, N.G., Fradkov, A.F., Terskikh, A., Matz, M.V., Labas, Y.A., Martynov, V.I., Yanushevich, Y.G., Lukyanov, K.A., and Lukyanov, S.A. (2001). GFP-like chromoproteins as a source of far-red fluorescent proteins. FEBS Lett. *507*, 16–20.

Ho, S.N., Hunt, H.D., Horton, R.M., Pullen, J.K., and Pease, L.R. (1989). Site-directed mutagenesis by overlap extension using the polymerase chain reaction. Gene *77*, 51–59.

Hoffman, R.M. (2008). Recent advances on in vivo imaging with fluorescent proteins. Methods Cell Biol. *85*, 485–495.

Hosoi, H., Mizuno, H., Miyawaki, A., and Tahara, T. (2006). Competition between energy and proton transfer in ultrafast excited-state dynamics of an oligomeric fluorescent protein red Kaede. J. Phys. Chem. B *110*, 22853–22860.

Kogure, T., Karasawa, S., Araki, T., Saito, K., Kinjo, M., and Miyawaki, A. (2006). A fluorescent variant of a protein from the stony coral *Montipora* facilitates dual-color single-laser fluorescence cross-correlation spectroscopy. Nat. Biotechnol. *24*, 577–581.

Lakowicz, J.R. (1999). Principles of Fluorescence Spectroscopy (New York: Kluwer Academic, Plenum Publishers).

Mena, M.A., Treynor, T.P., Mayo, S.L., and Daugherty, P.S. (2006). Blue fluorescent proteins with enhanced brightness and photostability from a structurally targeted library. Nat. Biotechnol. *24*, 1569–1571.

Merzlyak, E.M., Goedhart, J., Shcherbo, D., Bulina, M.E., Shcheglov, A.S., Fradkov, A.F., Gaintzeva, A., Lukyanov, K.A., Lukyanov, S., Gadella, T.W., and Chudakov, D.M. (2007). Bright monomeric red fluorescent protein with an extended fluorescence lifetime. Nat. Methods *4*, 555–557.

Nguyen, A.W., and Daugherty, P.S. (2005). Evolutionary optimization of fluorescent proteins for intracellular FRET. Nat. Biotechnol. *23*, 355–360.

Niwa, H., Inouye, S., Hirano, T., Matsuno, T., Kojima, S., Kubota, M., Ohashi, M., and Tsuji, F.I. (1996). Chemical nature of the light emitter of the *Aequorea* green fluorescent protein. Proc. Natl. Acad. Sci. USA *93*, 13617–13622.

Ohashi, T., Galiacy, S.D., Briscoe, G., and Erickson, H.P. (2007). An experimental study of GFP-based FRET, with application to intrinsically unstructured proteins. Protein Sci. *16*, 1429–1438.

Patterson, G.H., Piston, D.W., and Barisas, B.G. (2000). Förster distances between green fluorescent protein pairs. Anal. Biochem. *284*, 438–440.

Patterson, G., Day, R.N., and Piston, D.W. (2001). Fluorescent protein spectra. J. Cell Sci. *114*, 837–838.

Pedelacq, J.D., Cabantous, S., Tran, T., Terwilliger, T.C., and Waldo, G.S. (2006). Engineering and characterization of a superfolder green fluorescent protein. Nat. Biotechnol. *24*, 79–88.

Petersen, J., Wilmann, P.G., Beddoe, T., Oakley, A.J., Devenish, R.J., Prescott, M., and Rossjohn, J. (2003). The 2.0-Å crystal structure of eqFP611, a far red fluorescent protein from the sea anemone *Entacmaea quadricolor*. J. Biol. Chem. *278*, 44626–44631.

Quillin, M.L., Anstrom, D.M., Shu, X., O'Leary, S., Kallio, K., Chudakov, D.M., and Remington, S.J. (2005). Kindling fluorescent protein from *Anemonia sulcata*: dark-state structure at 1.38 A resolution. Biochemistry *44*, 5774–5787.

Remington, S.J. (2006). Fluorescent proteins: maturation, photochemistry and photophysics. Curr. Opin. Struct. Biol. *16*, 714–721.

Shaner, N.C., Campbell, R.E., Steinbach, P.A., Giepmans, B.N.G., Palmer, A.E., and Tsien, R.Y. (2004). Improved monomeric red, orange and yellow fluorescent proteins derived from *Discosoma* sp. red fluorescent protein. Nat. Biotechnol. *22*, 1567–1572.

Shaner, N.C., Steinbach, P.A., and Tsien, R.Y. (2005). A guide to choosing fluorescent proteins. Nat. Methods *2*, 905–909.

Shaner, N.C., Patterson, G.H., and Davidson, M.W. (2007). Advances in fluorescent protein technology. J. Cell Sci. *120*, 4247–4260.

Shaner, N.C., Lin, M.Z., McKeown, M.R., Steinbach, P.A., Hazelwood, K.L., Davidson, M.W., and Tsien, R.Y. (2008). Improving the photostability of bright monomeric orange and red fluorescent proteins. Nat. Methods *5*, 545–551.

Shu, X., Shaner, N.C., Yarbrough, C.A., Tsien, R.Y., and Remington, S.J. (2006). Novel chromophores and buried charges control color in mFruits. Biochemistry *45*, 9639–9647.

Verkhusha, V.V., Chudakov, D.M., Gurskaya, N.G., Lukyanov, S., and Lukyanov, K.A. (2004). Common pathway for the red chromophore formation in fluorescent proteins and chromoproteins. Chem. Biol. *11*, 845–854.

Wilmann, P.G., Petersen, J., Pettikiriarachchi, A., Buckle, A.M., Smith, S.C., Olsen, S., Perugini, M.A., Devenish, R.J., Prescott, M., and Rossjohn, J. (2005). The 2.1A crystal structure of the far-red fluorescent protein HcRed: inherent conformational flexibility of the chromophore. J. Mol. Biol. *349*, 223–237.

Yarbrough, D., Wachter, R.M., Kallio, K., Matz, M.V., and Remington, S.J. (2001). Refined crystal structure of DsRed, a red fluorescent protein from coral, at 2.0Å resolution. Proc. Natl. Acad. Sci. USA *98*, 462–467.

 ©2008 Elsevier Ltd All rights reserved